Annales Geophysicae

A numerical study of orographic forcing on TC Dina (2002) in South West Indian Ocean

S. Jolivet[1,2]**, F. Chane-Ming**[1]**, D. Barbary**[1]**, and F. Roux**[3]

[1]Laboratoire de l'Atmosphère et des Cyclones, UMR 8105 CNRS – Météo-France – Université de la Réunion, 15 avenue René Cassin, CS 92003, 97744 Saint Denis Cedex 9, Ile de la Réunion, France
[2]Singapore-Delft Water Alliance, National University of Singapore, 1 Engineering Drive 2, Blk E1, #08-25, 117576 Singapore, Singapore
[3]Laboratoire d'Aérologie, UMR 5560 CNRS – Université Paul Sabatier, 14 avenue Edouard Belin, 31400 Toulouse, France

Correspondence to: S. Jolivet (bohux@yahoo.fr)

Abstract. Using the French non-hydrostatic mesoscale numerical model Méso-NH, intense tropical cyclone (TC) Dina (2002) is simulated to investigate the forcing caused by the steep orography of Réunion island (20.8° S, 55.5° E) in the southwest Indian Ocean. The model initialised by a bogus vortex derived from Doppler radar observations reproduces quite well the dynamical characteristics of TC Dina approaching the island and provides some clues on the orographic influence on the structure and the evolution of the TC.

The presence of the island is observed to stabilise the cyclonic circulation by damping the natural elliptical eyewall rotation and forcing the flow circulation. Initially, the cyclonic flow is blocked upwind of the orography which induces a convergence associated with upward vertical velocities, intense precipitation and maximum horizontal winds along the upwind slopes of the island. A mountain wave, generated over the highest terrains, is associated with downward motions on the lee side. When the strongest winds reach the island, the flow changes its behaviour from passing around to over the island. Non-dimensional flow parameters in agreement with recent theories are calculated to explain TC track.

Keywords. Meteorology and atmospheric dynamics (Convective processes; Precipitation; Tropical meteorology)

1 Introduction

Tropical cyclones (TCs) are highly dangerous meteorological phenomena, especially for islands and coastal regions. They are the most exposed regions and so can endure strong winds, heavy rains causing flooding or storm surge. Research on TC approaching mountainous islands has received much attention, especially because many observations show evidence of the possible strong influence of the topography on TC dynamics which makes TC forecasting difficult (track, intensity, rainfall).

Several numerical modelling studies have previously focused on the orographic influence of islands on TCs. Brand and Blelloch (1973) showed that the average intensity of TCs crossing the Philippines decreases by 33 %, their propagation deviates northward and the circulation size of weak typhoons decreases substantially. Hebert (1980) discussed the deflection in the path of Hurricane David (1979) and Tropical Storm Frederic (1979) as they approached the mountainous island of Hispaniola in the Caribbean from the south. Bender et al. (1987) focused on the influence of mountainous islands which were shown to affect the basic flow field, to cause changes in track and translation speed, and to induce modifications in the structure of idealised TCs when making landfall on different mountainous islands such as Hispaniola, Taiwan and Luzon in the Philippines. Numerical experiments also revealed important effects of the mountainous terrain of Japan on TC making landfalls (Bender and Kurihara, 1987). In order to explain some observed tracks of TCs making landfalls on the east coast of Mexico, Zehnder and Reeder

(1993) studied the induced southward deflection in the case of an idealised vortex approaching a large scale mountain range from east.

Many studies have dealt more specifically with the influence of Taiwan whose Central Mountain Range (CMR), a north–south oriented 400 km × 120 km barrier of more than 3000 m elevation, is a major obstacle to cyclone track. It also induces significant variations in TC wind structures and precipitation (Pan et al., 2008; Lin et al., 2011). Wang (1980) made a compilation of all cyclones that affected Taiwan and divided them in two categories. The strongest ones tend to pass over the island with a continuous and cyclonically curved track, whereas the weakest ones have a discontinuous trajectory and dissipate on the eastern upwind side while secondary lows may form on the lee side. In an idealised numerical study at 60 km resolution, Chang (1982) represented the CMR of Taiwan as a rectilinear mountain range with a maximum altitude of 2000 m. The flow is shown to pass preferentially around the Island. The low level circulation is blocked by the CMR which induces a cyclonic curvature of the track. Also the propagation of TCs without sustained circulation is shown to be strongly dependent on the perturbation of the low level flow. In addition, Yeh and Elsberry (1993) show that deflection is larger for weak and slow cyclones whereas intense and fast cyclones pass across the island with a more continuous track, in agreement with Wang (1980). At the same time, Chang et al. (1993) showed that the development of a secondary low was linked to the presence of the TC centre in a specific area including southeastern Taiwan region and the ocean area to the east-southeast of it. Wu and Kuo (1999) gave an updated detailed overview of cyclones passing over Taiwan focusing on different characteristics such as track deflection, intensity changes, development of secondary lows and occurrence of different flow regimes.

Wu et al. (2003) showed that, when Typhoon Zeb (1998) made landfall on Luzon (Philippines), its eyewall contracted, then weakened and dissipated, before it reformed when the storm returned to the ocean. The weakening of the storm was likely due to surface friction and water vapour cut-off, while the outer circulation was less affected. Lin et al. (2005) determined six non-dimensional parameters controlling the importance of orographically induced deviation of the cyclone track. Using idealised simulations it was shown that a strong (weak) orographic blocking impacting a weak (strong) TC induced a discontinuous (continuous) track. Recently, this conceptual model was applied by Lin et al. (2006) to the case of Toraji (2001), a typhoon of moderate intensity with a discontinuous track, and to Bilis (2000), a super-typhoon with a continuous track. Results from the non-dimensional control parameters calculated for both cyclones are consistent with the theory. An intense storm will have a continuous track because of weak blocking effect of the CMR, whereas a weak storm will have its propagation stopped by the CMR. Through a sensitivity study with lowered Taiwan terrain el-

evations, Jian and Wu (2008) showed that the channelling of low-level flow between the storm core of supertyphoon Haitang (2005) and the mountains controls southward track deflection and loop amplitude. Backward trajectory analyses from the high resolution simulations of Typhoon Krosa (2007) support also the concept of the looping motion being influenced by the channelling effect (Huang et al., 2011). In addition, Yeh et al. (2011) showed that the channelling effect is not a necessary condition for the looping motion. Recently from a dataset of 131 TCs crossing Taiwan, Peng et al. (2012) constructed a statistical model based on 3 most influential parameters – landfall location, maximum wind and approaching direction – for diagnosing TC track continuity with more than 80 % accuracy.

Recently Chambers and Li (2011) investigated the effect of Hawaii's Big Island (BI) on TC. They showed that Hawaii's BI slows the track of approaching storms because of low tropospheric flow blocking and then induces southward deviation. Structural and track changes such as axisymmetrisation for storm passing very close to Hawaii's BI were observed. For storms passing to the south of Hawaii's BI a deviation on the right occurs. Finally they showed that in the wake of the island stronger intensities can result from weakened vertical wind shear.

Concerning the southwestern Indian Ocean (SWIO), Padya (1975) and Hoarau (2001) discussed the observed topography induced variability of winds during cyclonic conditions, which were recorded by surface stations in Mauritius and Rodrigues Islands, respectively. In this basin, Réunion island (20.8° S, 55.5° E) has a higher topography with a nearly elliptical form (70 km northwest–southeast, 50 km northeast–southwest) and a roughly conical shape with its highest point, Pîton des Neiges, at 3071 m above sea level in its central part. In comparison Taiwan and Hawaii's BI are similar to a large rectangular shaped barrier (400 km × 120 km, highest altitude 3952 m) and a wide high cone (129 km × 150 km, highest altitude 4205 m), respectively (Chamber and Li, 2011). Located in the third most active TC basin, Réunion island is also famous for holding several rainfall world records (accumulated during 12 h to 15 days), all established during the passage of a TC near the island, e.g., Hyacinthe (1980) and Gamede (2007) (Quetelard et al., 2009). Roux et al. (2004) analysed the kinematic structure and evolution of the TC Dina (2002) in the southwest Indian Ocean (SWIO) when it passed close to Réunion island, applying the Ground Based – Extended Velocity Track Display (GB-EVTD) method to Doppler radar observations. The analysis suggested some orographic effects of the island on TC Dina dynamics.

In the present study, numerical experiments are performed to investigate TC Dina when it approached Réunion island. This paper is organised as follows: Sect. 2 provides a short description of TC Dina, Sect. 3 concerns the modelling framework, Sect. 4 describes simulated storms with comparisons to observations, Sect. 5 focuses on the inner
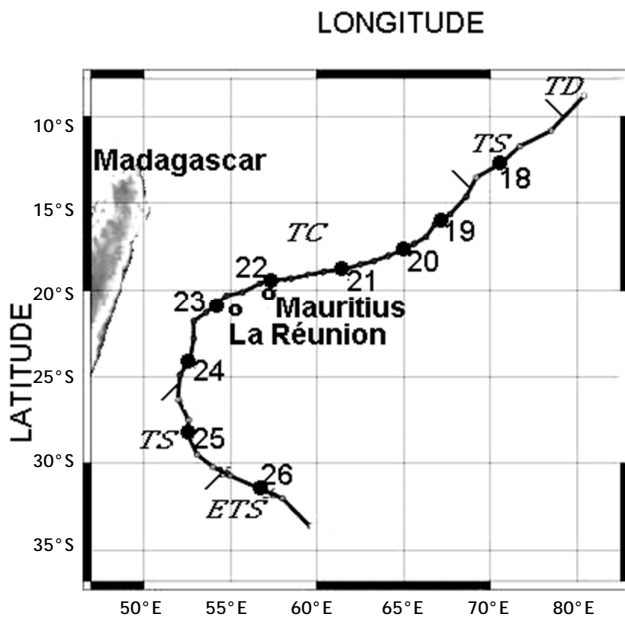
Fig. 1. Track of intense tropical cyclone Dina from 17 til 26 January 2002; symbols TD, TS, TC, and ETS denote tropical depression, tropical storm, tropical cyclone, and extratropical storm stages (adapted with permission from RSMC La Réunion/Météo-France).

Fig. 2. Accumulated rainfall (shaded contours, mm) and wind direction (arrows) for wind maxima (km h^{-1}) observed in Réunion island from 00:00 UTC on 22 January 2002 to 00:00 UTC on 23 January 2002 (adapted with permission from RSMC La Réunion/Météo-France).

core dynamics, and a discussion on control parameters is finally presented in Sect. 6 followed by concluding remarks in Sect. 7.

2 Intense tropical cyclone Dina (2002)

Dina formed on 16 January 2002 from a large region of deep convection near Diego Garcia Island (8° S, 76° E) in the SWIO (Fig. 1). Following a very fast cyclogenesis phase, it became a tropical depression on the 17th while moving rapidly (>10 m s^{-1}) southwestward (Caroff and Quetelard, 2002). The storm was upgraded to tropical cyclone on the 18th by the Regional Specialised Meteorological Centre (RSMC) of Réunion island (Météo-France). From the 19th to the morning of the 20th, it intensified to an estimated maximum (10-min averaged) surface wind of 70 m s^{-1} and a minimum surface pressure of 910 hPa at its acme. Then, from the 20th to the 22nd, the maximum surface wind and mean sea level pressure weakened to 60 m s^{-1} and 920 hPa, respectively. Dina passed near Mauritius Island at 23:15 UTC on the 21st, with a minimum distance of 65 km between the storm centre and the northern tip of the island. At this time, the diameter of the eye was about 85 km.

Fortunately, its track deviated slightly westward thereafter, and Dina came close to the coasts of Réunion island between 10:00 and 18:00 UTC on the 22nd with a minimum distance being of 65 km between the storm centre and the northwestern coast. Roux et al. (2004) suggested the possi-
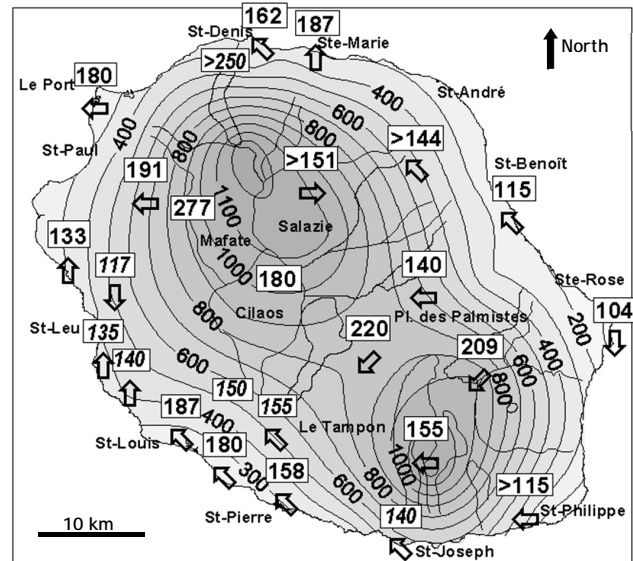
ble influence of the topography on the track deflection. At this time, the eyewall was relatively symmetric and the diameter of the eye was about 65 km. The strongest winds and highest reflectivity values derived from the Doppler radar data (Roux et al., 2004) were found at 40 to 60 km from the storm centre, at some distance from the coast, which spared the island from more dramatic damage. Nevertheless, strong winds were observed: gusts >50 m s^{-1} on the coastal regions and >55 m s^{-1} over the elevated zones (Fig. 2). The duration of these strong winds was also long: 24 h of wind gusts over 25 m s^{-1}. Heavy rains were also observed: rain rates >50 mm h^{-1} during more than 12 h and 500–2000 mm accumulated in 72 h (Fig. 2), especially in the inner part of the island where the terrain is high. The steep orography of Réunion island certainly played an important role in the location and intensity of strong winds and heavy rain. Flooding due to run-off and high storm surge of 6 to 9 m height also caused major damages, mostly in the northern coastal regions. A consequence of the very strong winds was the destruction of the Météo-France Doppler weather radar at 14:22 UTC on 22 January 2012.

Dina was one of the strongest cyclones reaching Réunion island over the last 40 years. The extent of damages was attributed to its relatively slow motion. A nearly constant propagation speed of 6.0 to 6.3 m s^{-1} when Dina was close to the island was deduced from the radar observations, while its track was southwest between 06:00 and 12:00 UTC before shifting to west with a west-southwest direction between 12:00 and 18:00 UTC. Similar deviations have been
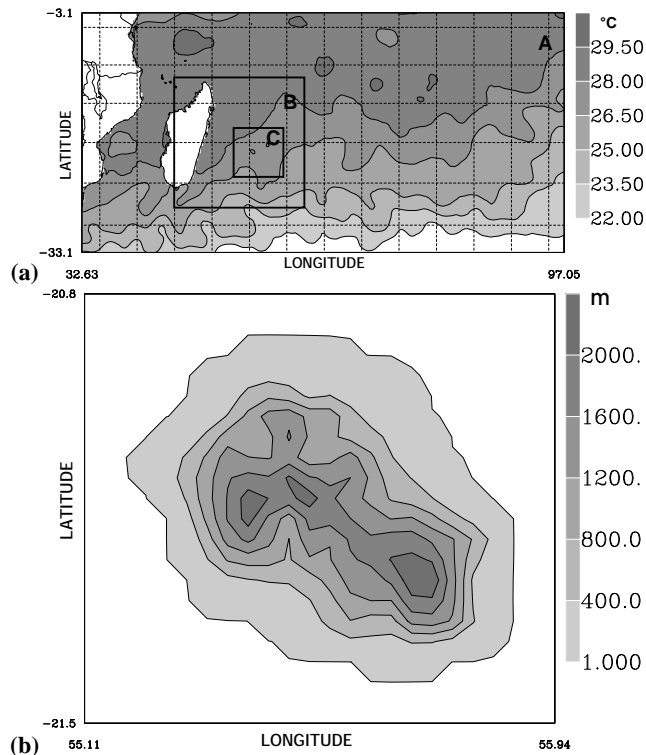
Fig. 3. (a) Configuration of the three nested domains and sea surface temperature (shaded, °C) on 22 January 2002. Domain A has 200 × 100 grid points with 36 km grid resolution, domain B has 162 × 162 grid points with 12 km grid resolution, and domain C has 180 × 180 grid points with 4 km grid resolution; **(b)** Orography of Réunion island in domain C (m).

observed for some TCs passing at a relatively close distance from Réunion island, such as Florine (1981). On the 23rd, Dina's track changed to south direction and its intensity started to decrease rapidly: 55 m s^{-1} and 925 hPa on the 23rd at 00:00 UTC, 45 m s^{-1} and 955 hPa on the 24th, 25 m s^{-1} and 985 hPa on the 25th. It then became very asymmetric and was carried along the westerly mid-latitude circulation as an extra-tropical depression. The stratosphere was also impacted by the passage of Dina close to Réunion island. Indeed Chane Ming et al. (2010) observed a large production of convective inertia-gravity waves in the lower stratosphere above TC Dina from 21 to 23 January 2012 in good correlation with the TC dynamics during its passage close to Réunion island e.g., intense TC.

3   Numerical simulation framework

Two numerical experiments were conducted to quantify the influence of the island on a cyclone: the first one – referred to as "*Island*" – used the real orography of the island, whereas in the second one – referred to as "*Ocean*" – Réunion island was replaced by ocean. Both simulations lasted 33 h

and they were initialised at 00:00 UTC, 22 January 2002, with 12-hourly lateral boundary conditions (including the Sea Surface Temperature, SST) from operational analyses of the European Centre for Medium-range Weather Forecast (ECMWF).

The French non-hydrostatic mesoscale numerical model Méso-NH, developed by Centre National de Recherches Météorologiques (Météo-France) and Laboratoire d'Aérologie (Université de Toulouse and Centre National de la Recherche Scientifique) (Lafore et al., 1998), is described and available at http://mesonh.aero.obs-mip.fr/mesonh/. The simulations were run using the M4.3B1 version with a "bogus vortex" package, and three nested domains A, B, C at 36, 12 and 4 km horizontal resolution, with 200 × 100, 162 × 162 and 180 × 180 grid points, respectively (Fig. 3a). Figure 3b represents the orography of Réunion island in the 4 km resolution domain. The spatial distribution is realistically reproduced with 2 highest peaks of Pîton Neiges (3071 m) in the central region and a third one associated with Pîton de la Fournaise (2632 m) in the south region. Nevertheless, the maximum mountain height used in the model is 571 m lower than the actual height of Pîton des Neiges with a maximum altitude of 2500 m.

Sixty levels with the Gal-Chen and Sommerville (1975) terrain-following coordinate are set with a vertical spacing varying from 50 m for the first level above the surface to 1 km at the top of the domain, at 21 km altitude. The upper boundary condition (last five levels) is made of a numerical "damping layer" preventing spurious reflection of gravity waves. In addition to a parameterisation of shallow convection, domains A and B use parameterised convection (Kain and Fritsch, 1990, 1993), C explicitly resolves deep convection. ECMWF radiative fluxes (Morcrette, 1989), Interactions Soil-Biosphere-Atmosphere (ISBA, Noihlan and Planton, 1989) surface fluxes with the Charnock (1955) formulation, microphysics with 5 classes of hydrometeors (cloud, rain, ice crystals, snow, graupel) (Caniaux et al., 1995), one-dimensional turbulence scheme (Bougeault and Lacarrère, 1989; Cuxart et al., 2000) are used for all domains. The SST is not a prognostic variable of the model, it evolves only as a boundary condition every 12 h. The two-way grid-nesting technique allows the three domains to exchange information: domain A (respectively B) imposes boundary conditions to domain B (respectively C). In the overlapping zone, the fields from the higher resolution domain are provided for the lower resolution one.

Assimilating coastal Doppler radar data in numerical weather prediction models shows very encouraging improvements in TC forecasting during landfall (Zhao et al., 2012). Here the RDVC (*Radar and Dropwindsonde Vortex Conditioning*) technique is used to initialise Méso-NH (Nuissier et al., 2005). First the ill-defined and ill-located cyclonic vortex is extracted from the large-scale ECMWF analysis. Then it is replaced at a specific location given by the best track, by a more realistic balanced (i.e., wind and temperature fields

in thermal wind equilibrium) vortex derived from the radar observations.

First, the Kurihara et al. (1993, 1995) filtering technique is applied to the large scale ECMWF field at 00:00 UTC on 22 January 2002. This large scale analysis is composed of a "basic field" and a "disturbance field" which are separated using a Barnes (1964) filter. The disturbance field is composed of a "non-vortex" part and a "vortex" part. Separating these two parts, then adding the "basic field" to the "non-vortex" part provides the "environmental field" filtered from any spurious vortex influence. The cyclone centre is determined by the minimum of wind and the filtering is made inside the region where the tangential wind is larger than $6\,\mathrm{m\,s^{-1}}$. Then, an analytic symmetric "bogus vortex", deduced from the GB-EVTD analysis on the Doppler radar data from 10:22 to 11:22 UTC on 22 January 2002 (Roux et al., 2004), is added to the "environmental field" at 00:00 UTC on 22 January 2002. The observations show that from 00:00 to 12:00 UTC the cyclone is quasi-steady in terms of intensity and structure, so we can suppose that the radar observations are representative of the earlier cyclone structure. The bogus vortex has a maximum tangential wind of $65\,\mathrm{m\,s^{-1}}$ at $50\,\mathrm{km}$ from its centre. It extends to a radius of $600\,\mathrm{km}$, which corresponds to the mean radius of the "vortex disturbance" in the ECMWF analysis. This vortex is initially equilibrated by the thermal wind equation and the moisture field is taken from the ECMWF analysis.

In our case, an initial spin-up period of $9\,\mathrm{h}$ during which the model adapts to the included bogus vortex was observed (Nuissier et al., 2005). The period during which the simulated storm interacts with the island orography, that is to say when the centre of the vortex is located at less than $100\,\mathrm{km}$ from the island coast, lasts between 15 and 24 h of simulated time. Thus, at this time, possible spurious effects induced by the spin-up are minor.

4   Characteristics of the simulated storms

Figure 4 shows Dina's best track and the simulated trajectories from the initial point at 00:00 UTC on 22 January 2002, when the cyclone was located about 50 km north of Mauritius (the simulated tracks are computed using the minimum of sea level pressure (MSLP) with an error of less than 1 km). The simulated storms from the "*Ocean*" and "*Island*" experiments move west-southwest during the next 6 h before shifting to southwest. The observed centre is located about 100 km north of Réunion island at 12 h. After 00:00 UTC on the 23rd, Dina's track deviated toward south-southwest. At the closest point to Réunion island both simulated tracks are 50 km south of the best track, at approximately half the observed distance. The tracks change when the storm approaches Réunion island, but with different timing. For "*Ocean*", the track direction is almost constant toward southwest during 33 h with a quasi-linear track and no
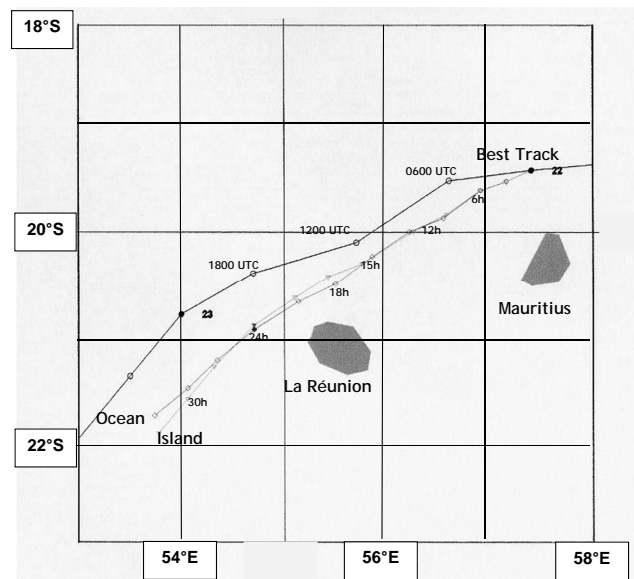

Fig. 4. Best track of tropical cyclone Dina (circles) and simulated tracks from the two numerical experiments ("*Island*" experiment: triangles, "*Ocean*" experiment: squares) from 00:00 UTC on 22 January 2002.

change in the propagation speed. For "*Island*", the track direction shows a slight westward deflection between 15 and 24 h, and a southward one thereafter. Nevertheless during the 33 h of simulation, the difference between the "*Ocean*" and "*Island*" tracks described above is less than 10 km, in the range of model uncertainty. Thus, the impact of the island on the track is hardly detectable, even though the simulated storms are closer to the island and the orographic effect should have been enhanced. Moreover, due to the initial spin-up time, the simulated storms are relatively late compared to the observed one. For this reason the period during which TC Dina interacts with the island is delayed by a few hours.

Evolution of the maximum wind at 1 km altitude is quite similar in both experiments before the simulated storm begins to interact with the island (Fig. 5a). After initialisation with the balanced vortex through the RDVC technique, the simulated storm weakens during the first 6 h then re-intensifies (spin-up period). Then the simulated wind reaches a maximum of $73\,\mathrm{m\,s^{-1}}$ at 15 h in both experiments before diverging afterwards. The maximum winds in "*Ocean*" are constantly stronger than in "*Island*". Figure 5b also shows that the minimum sea level pressure (MSLP) is similar for both experiments until 15 h before diverging afterwards with "*Ocean*" MSLP being lower than "*Island*" MSLP. Based on these results, we define the interaction period which lasts from 15 to 24 h. During this period the presence of the island slows the intensification process of the TC and, thus, induces a less intense TC in "*Island*" compared to "*Ocean*".

Figure 5c presents the ratio between the major and minor axes of the elliptical eye from 14 to 27 h of simulated time.
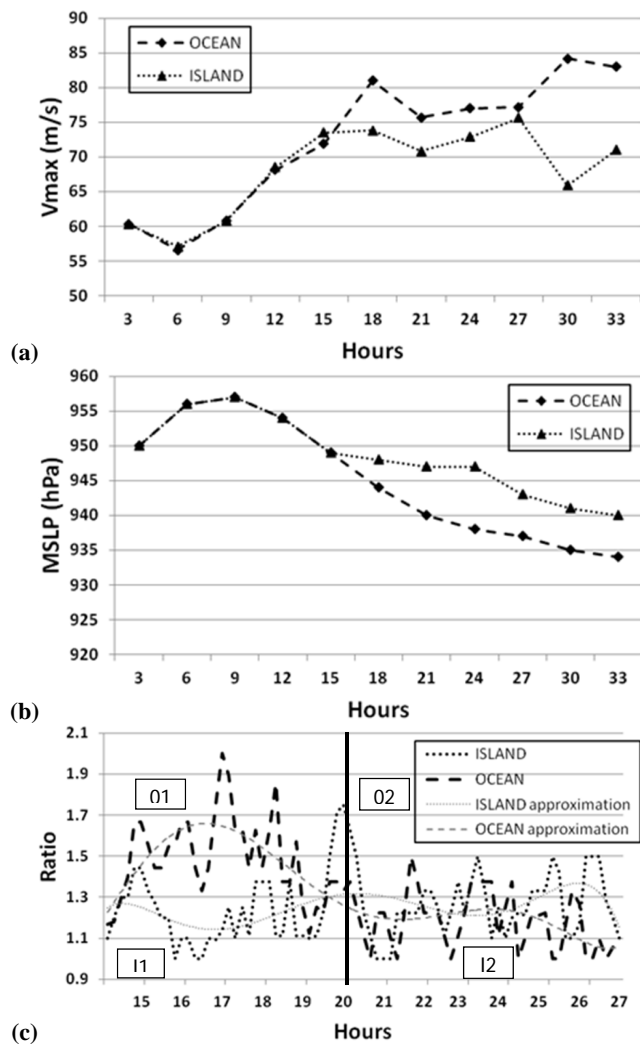
Fig. 5. (a) Time series of the maximum wind velocity (m s^{-1}) at 1000 m altitude for the "*Ocean*" and "*Island*" from 3 to 33 h (at 3-h interval); **(b)** as in **(a)**, except for minimum sea level pressure (MSLP) (hPa); **(c)** as in **(a)**, except for the ratio between major and minor axes of the eye from 14 to 27 h (1 h interval). Grey lines indicate trend of the ratio (polynomial approximation, 6th order).

Fig. 6. (a) Observed Doppler velocity values (m s^{-1}) at 0.5° elevation at 14:22 UTC on 22 January 2002; **(b)** Doppler velocity values (m s^{-1}) deduced from the "*Island*" experiment at 17:30 at 1000 m altitude. Symbol "R" indicates the location of the Doppler radar, the dashed line contour indicates the location of Réunion island, negative values (away from the radar) are shaded.

These axes are defined at 1 km altitude by analysing the contour of 45 m s^{-1} wind intensity in the eyewall. In "*Island*" the mean ratio is about 1.2, which corresponds to a quasi circular shape during the whole period beside around 20 h. Indeed from 19:30 to 20:30 "*Island*" displays an elliptical shape. Actually this happens when the TC is close to the island coasts with the cyclonic circulation hitting perpendicularly the ridge of the island. In this configuration the ridge of the island efficiently blocks the low-level flow. In "*Ocean*" from 15 to 20 h, the ratio is about 1.6 corresponding to a well-defined elliptical shape, and then decreases to about 1.2 from 20 to 27 h. It has to be noticed that, during the whole period, both simulations show faster fluctuations of the eye shape with a period of approximately 45 min, superimposed to the mean
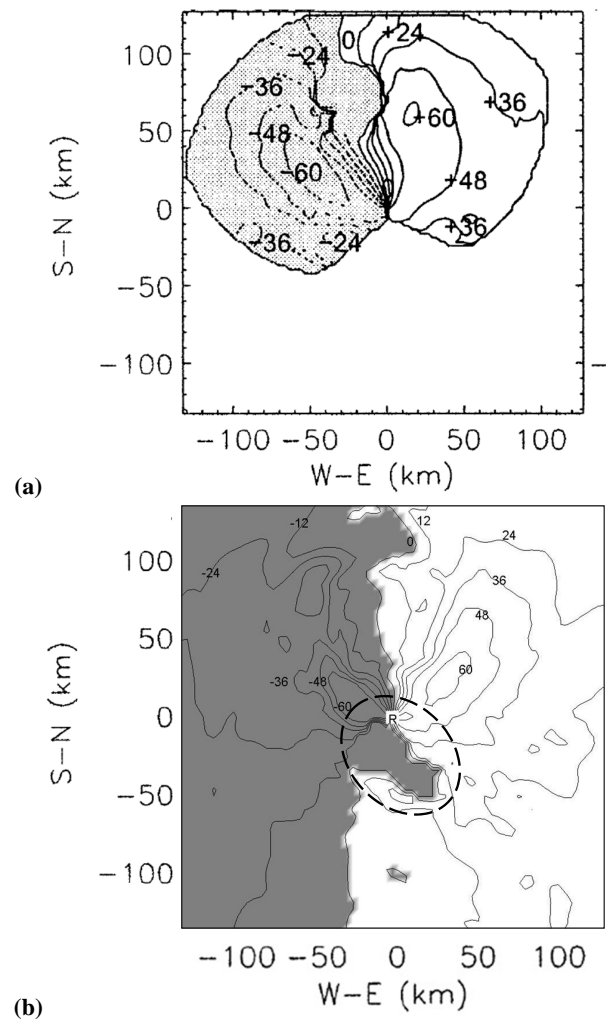
tendencies. These faster oscillations are in good correlation with the natural behaviour of a TC which usually displays relatively small fast variations of the eye size (Braun, 2002; Oda et al., 2006).

The reliability of the results from the "*Island*" simulation during the final approach can be evaluated through a comparison with the radar observations up to 120 km north of the island. Figure 6 shows the observed Doppler velocities at 14:22 UTC on 22 January at 0.5° elevation and the simulated ones in "*Island*" at 17:30 of simulated time at 1000 m altitude. Except for the time difference of 3 h, observed and simulated fields are quite similar. The intensities rise up to more than ± 60 m s^{-1} in the part of the eyewall region where the radar beam and the wind direction are parallel. It can also be
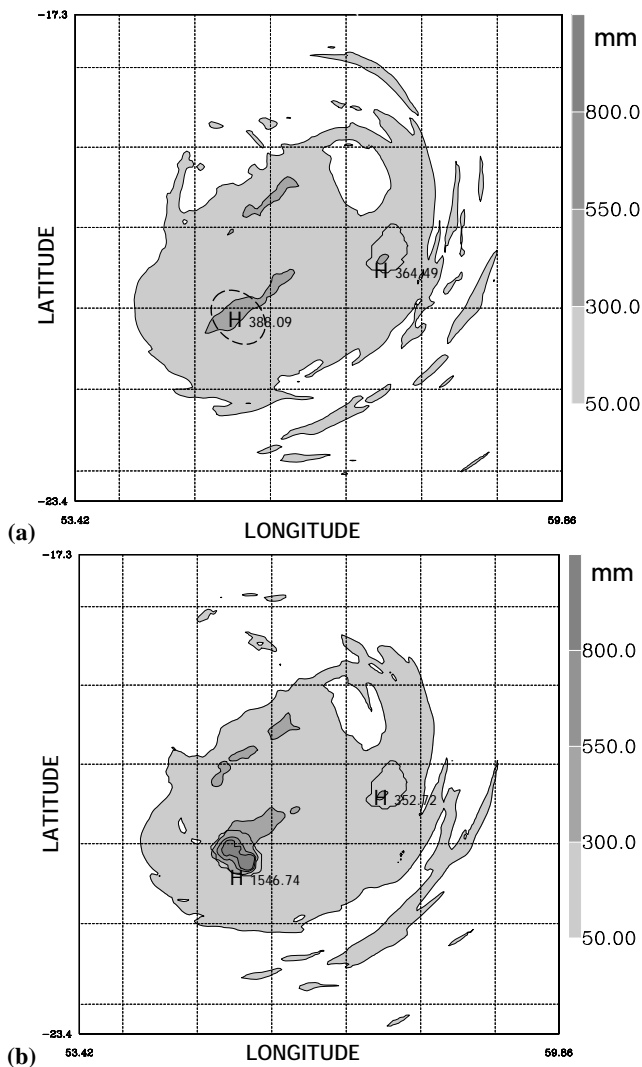
Fig. 7. (a) 24 h accumulated rainfall from 0 to 24 h (shaded, mm) for *"Ocean"*. The dashed line contour indicates the location of Réunion island in *"Ocean"*; **(b)** as in **(a)**, except for *"Island"*.

noted that the simulated and observed Doppler velocities display similar asymmetry with slightly stronger negative than positive values in the left part of the domain.

In both simulations, the 24 h accumulated precipitation pattern is parallel to the track (Fig. 7). More precisely, relatively low precipitation values are located along the path of the simulated cyclone centre. To the right and to the left relatively to the storm motion at a distance of about 50 km of this simulated centre, large amounts of accumulated rain are observed due to the heavy rainfall in the eyewall. These amounts are more widespread in the southern side (left), due to the convergence between the cyclonic circulation and the anticyclonic flow south of it (Caroff, 2002). The main precipitation patterns are similar for both experiments, except over and downstream of Réunion island. Due to the orographic amplification of precipitation, over Réunion island the maxi-

mum rain amount is much larger in *"Island"* (1546 mm) than in *"Ocean"* (388 mm). The amount simulated in *"Island"* is in good agreement with the observations which show maximum 24-h accumulated rain values larger than 1200 mm in the northern part of the island (Fig. 2). It has to be noted that the simulated vortex was closer to Réunion island in both experiments, inducing a relatively large amount of accumulated rain over this region in *"Ocean"*.

Southwest of Réunion island, *"Island"* is much drier than *"Ocean"*, with a deficit of rainfall downstream of the island, whereas the rainfall amount pattern is more continuous in *"Ocean"*. Although *"Island"* has a larger maximum (Fig. 7), the average amount of rainfall accumulated during 33 h in domain C (5.2×10^5 km^2) is almost identical in both experiments (64.71 mm for *"Ocean"* and 64.59 mm for *"Island"*). More precisely in domain C, during the period before interaction (0 to 15 h) *"Island"* produces 28.7 mm and *"Ocean"* 27.9 mm; during the period of interaction (15 to 24 h) *"Island"* produces 16.6 mm and *"Ocean"* 17.5 mm; and after interaction with the island (24 to 33 h) *"Island"* and *"Ocean"* produces 19.3 mm. Hence, the island modifies the spatial distribution of rainfall, but it does not influence the total amount.

Finally, Méso-NH is capable of simulating a realistic TC, in agreement with the observations of TC Dina in terms of rainfall, wind, intensity and structure. Due to the errors in track (both simulated tracks are similar and much closer to the island) a comparison between the simulations and real Dina is not relevant. Nevertheless, both simulations display significant differences during the interaction period (between 15 and 24 h) which can be used to investigate the forcing caused by the steep orography of the island on the inner core dynamics.

5 Inner core analysis of *"Ocean"* and *"Island"* experiments

We will now focus on the period when the centre of the simulated storm is less than 100 km from the island coast, between 15 and 24 h of simulated time. From the end of the initial spin-up time to the beginning of the interaction period, both simulations display very similar wind and precipitation fields (not shown). After 15 h, there are significant differences between the results from *"Ocean"* and *"Island"*, reflecting different characteristics of the inner core dynamics. Analysis of these differences provides information on some aspects of the orographically forced evolution of the TC.

5.1 *"Unperturbed"* evolution of the simulated storm

In *"Ocean"* experiment, two periods can be identified (Fig. 5c). The first one (period O1) lasts from 15 to 20 h, when all structures from the different fields are changing in relation with the rotation of an elliptical eyewall. The second one (period O2) lasts from 20 to 24 h, when the structures
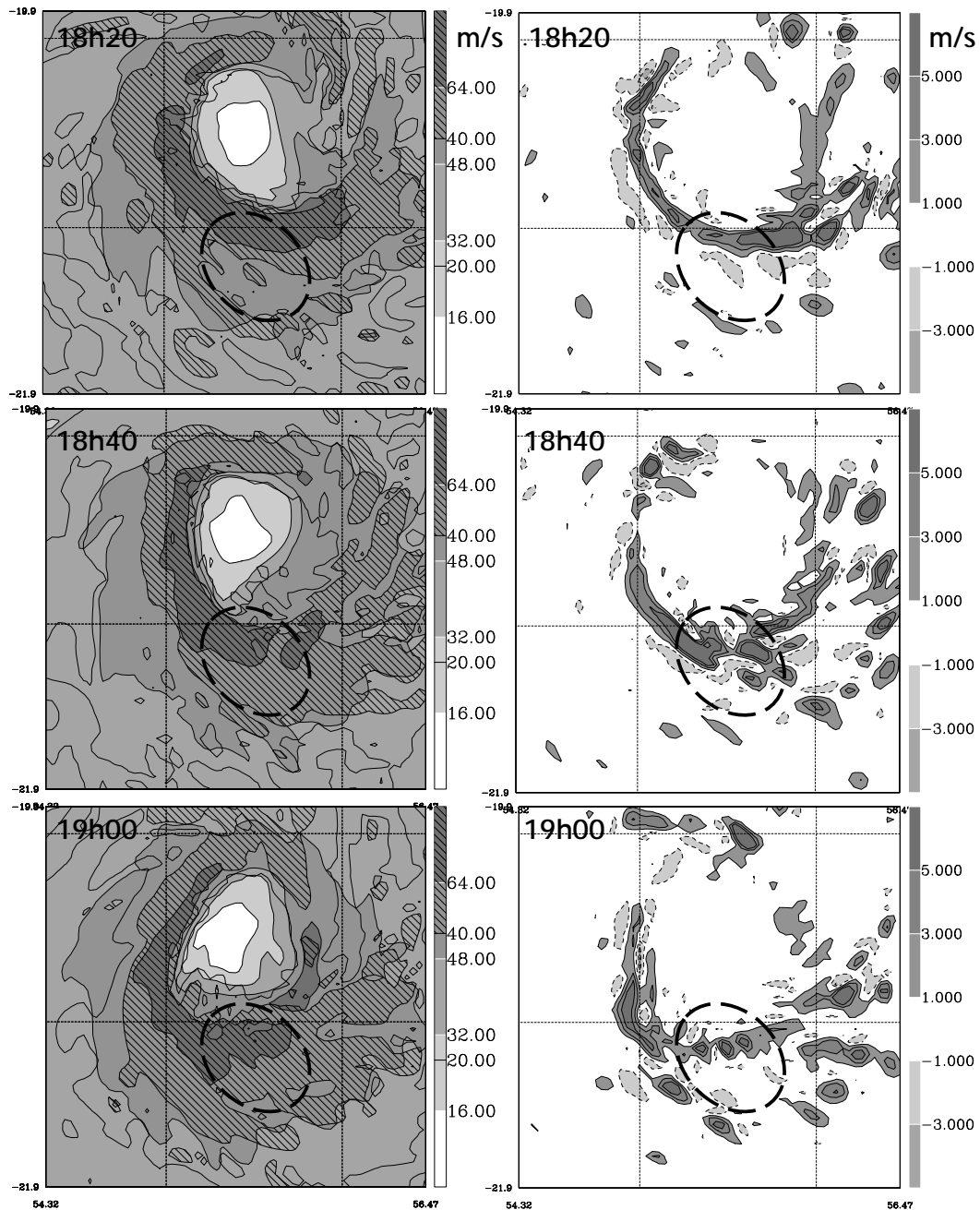
Fig. 8. Left panels: horizontal wind speed (shaded, m s^{-1}) and radar reflectivity (20 and 40 dBZ contours, hatched zones denote values >40 dBZ) from the 4-km model of experiment "*Ocean*" at 1000 m altitude, every 20 min from 18:20 to 19 h; right panels: as left panels, except for vertical velocity values (shaded, m s^{-1}) at 5000 m altitude. The dashed line contour indicates the location of Réunion island.

are steadier in relation with the rotation of a more circular eyewall. During O1, "*Ocean*" produces a cyclonically rotating elliptical eye with major and minor axes of about 95 and 55 km, respectively. At this time, the strongest winds are larger than 80 m s^{-1} in the eyewall and located 50 to 70 km away from the centre (Fig. 8). The major axis of the eye turns cyclonically (clockwise in the Southern Hemisphere) from southeast–northwest at 18:20 to southwest–northeast

at 19:00 h, with a rotation period of about 200 min. The strongest winds at 1000 m altitude from 18:20 to 19:00 h are in the southwestern half of the eyewall. The area of strong winds progressively extends to northwest and southeast with time. Also noteworthy is the intensification of the winds stronger than 40 m s^{-1} (up to 54 m s^{-1}) in the northeastern quadrant, in relation with the cyclonic expansion of the strong wind zones at a speed slightly faster than that of the
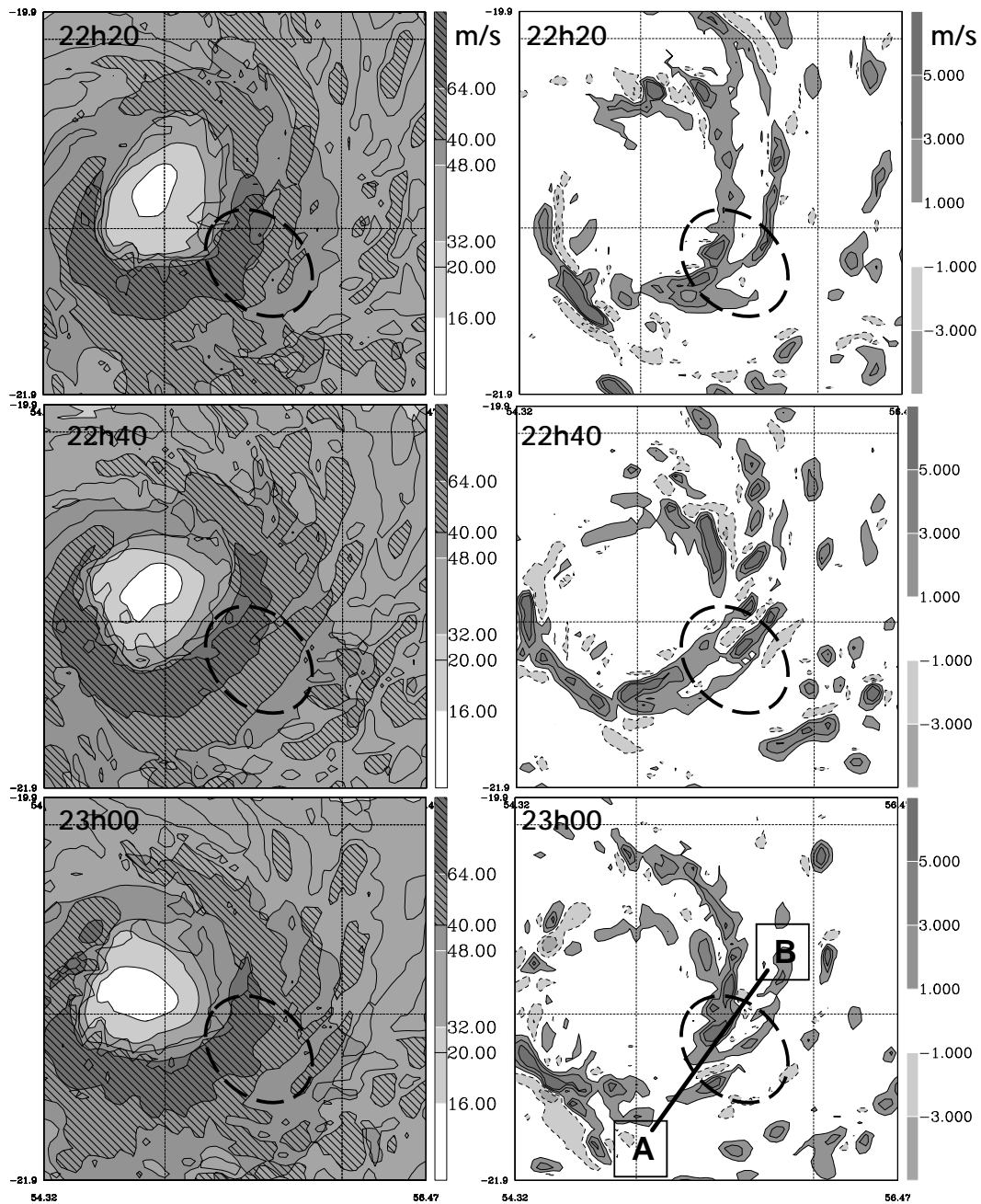
Fig. 9. As in Fig. 8, except for 22:20 to 23 h. Line AB in the lower right panel shows the location of the southwest–northeast vertical cross-section in Fig. 10.

eye rotation. The radar observations (Roux et al., 2004) show a similar evolution of the wind: at 2 km altitude, the location of the maximum wind changed from east at 10:52 UTC to south at 13:52 UTC. As a consequence of this axisymmetrisation process, the wind field in the eyewall becomes more homogeneous, though its south-eastern part remains more intense.

The reflectivity field at 1 km altitude shows a good correlation between the maximum values and the strongest hori-

zontal winds (Fig. 8). The precipitation structure of the eye is elliptical, but its shape is more complex than that associated with the wind field. The eyewall is not a continuous ring of intense precipitation around the eye, but rather a spiral band which converges clockwise from southeast to east. The location of the highest reflectivity values is well correlated with the maximum winds, but the region of most intense precipitation more clearly shows a southeast to southwest motion than the strong wind zone. Likewise, the clockwise extension of

the high reflectivity zone in the eyewall (from north at 18:20 to south-east at 19:00 h) is similar to that of winds stronger than $40 \, \text{m s}^{-1}$.

Regions of upward velocities (up to $5–6 \, \text{m s}^{-1}$, which is rather intense for an horizontal resolution of 4 km) at 5 km altitude are in agreement with areas of maximum reflectivity at 1 km altitude (Fig. 8). Also the high precipitation zones are extending clockwise in relation with the large cyclonic motion during the hydrometeor fall in the eyewall. Vertical velocity fields give a sharper picture of the active zones in the eyewall, making the time sequence of a rotating maximum more evident (southeast at 18:20, south at 18:40, southwest at 19:00 h). The discrete nature of the external spiral rainbands also appears with spots of high vertical velocities along them.

During the second period of "*Ocean*" (period O2), from 22:20 to 23:00 h, the eye has a less elliptical and more circular shape of similar size (Fig. 9). Its major axis is oriented from south–southwest to north–northeast at 22:20 and it rotates cyclonically to west–east at 23:00 h, which corresponds also to a rotation period of about 200 min. The maximum reflectivity values are also found in the southern part of the eyewall, but as observed for the strongest winds, this field is fairly steady (Fig. 9). The eyewall still has the form of a spiral band converging cyclonically from northeast to northwest. Maximum upward velocities are located in the southwest part of the eyewall (Fig. 9), in agreement with the high reflectivity zone, and its location is almost stationary during the considered period. A secondary maximum, located in the spiral rainband in the north-eastern part of the domain propagates downwind and progressively merges with the main maximum to the south of the eyewall.

The passage of the strongest winds over the location of Réunion island in "*Ocean*" is illustrated with a series of vertical southwest–northeast cross-sections from 18 to 24 h (Fig. 10). In relation with the previously discussed evolution of the eyewall, different maxima are observed. The strongest winds ($>64 \, \text{m s}^{-1}$) are located between 500 and 2500 m altitude and they are associated with convective precipitation characterised by relatively large vertical development. Precipitation then becomes more stratiform, as revealed by the presence of a "bright band" of strong reflectivity values near the level of the 0 °C isotherm at 4.5 km altitude, when these areas of convective precipitation are advected toward southwest by the cyclonic winds. The weaker maximum at 24 h, which is not directly associated with a region of strong horizontal wind, is related to the passage of an external spiral rainband.

5.2 Interaction between the simulated storm and the island

In "*Island*", two periods can be considered, showing different kinds of interaction with the orography. From 15 to 20 h (period I1), rotation of a less elliptical and more circular eyewall is still apparent but weaker than in "*Ocean*", probably

in relation with the orographic constraint on the horizontal flow. From 20 to 24 h (period I2), the horizontal circulation, vertical velocity and radar reflectivity fields are steadier associated with a circular shape of the eye.

During the first period (I1), from 18:20 to 19:00 h, the horizontal wind at 1 km altitude displays noteworthy characteristics (Fig. 11). Five striking features distinguish the "*Island*" results from the "*Ocean*" ones:

1. The eye is more circular in "*Island*", with major and minor axes of 85 and 75 km, respectively (compared to 95 and 60 km in "*Ocean*" in Fig. 8). It is also rotating cyclonically (clockwise), but with a slightly faster period of about 180 min (compared to 200 min in "*Ocean*") which is closer to the observed value of 150 min (Roux et al., 2004);

2. The area of strong winds ($>64 \, \text{m s}^{-1}$) is much smaller and stays at a fixed location between the cyclone centre and the north of Réunion island. This results from the channelling effect of the high terrains in the central part of the island (Jian and Wu, 2008);

3. The wind velocity is minimum on the leeward (southwestern) side of Réunion island;

4. The horizontal extension of the cyclone-force winds ($>32 \, \text{m s}^{-1}$) is slightly smaller than in "*Ocean*";

5. The circulation in the eyewall is more symmetric and the region of strong winds ($>48 \, \text{m s}^{-1}$) forms a closed annulus throughout the considered period, whereas it was closed only after 18:40 in "*Ocean*".

The strongest winds in the northern part of the island are associated with high reflectivity values (Fig. 11). The simulated precipitation is weaker on the downwind side of the island. Vertical velocity is in good correlation with the wind and reflectivity (Fig. 11). The strongest upward motions are also located to the north of the island, on the upwind side where the cyclonic flow hits the terrain. Another remarkable feature is the presence of downward vertical velocities in the downwind part of the island, interrupting the zone of intense upward motions in the southern and eastern part of the eyewall.

From 22:20 to 23:00 h (I2), the horizontal winds at 1 km altitude also display stationary features in relation with the strong orographic forcing induced by the presence of the island in the inner core circulation (Fig. 12). The eye still shows an almost circular shape, and rotates cyclonically with a longer period of 220 min. Two areas of strong winds ($>50 \, \text{m s}^{-1}$) are present. The narrow one, still located in the north-western part of Réunion island, results from the above mentioned channelling effect. The area of strong winds which progressively extends in the southwestern quadrant of the eyewall results from downstream convergence of
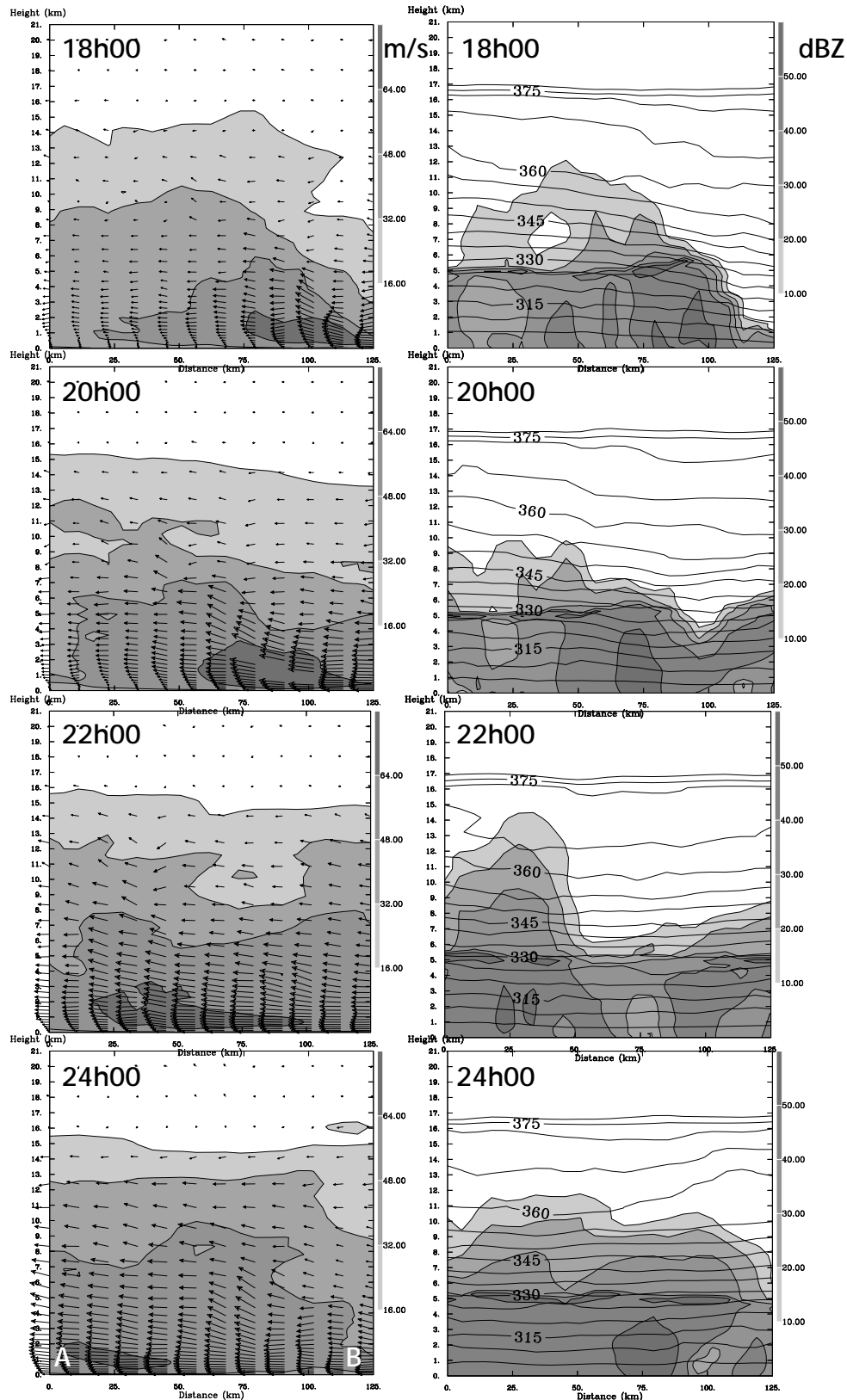
Fig. 10. Left panels: vertical cross-sections of horizontal wind speed (shaded, m s^{-1}) and wind vectors along line AB (see Fig. 9) in the 4-km model of experiment "*Ocean*", every 2 h from 18 to 24 h ; right panels: as left panels, except for radar reflectivity (shaded, dBZ) and potential temperature (contours, K).
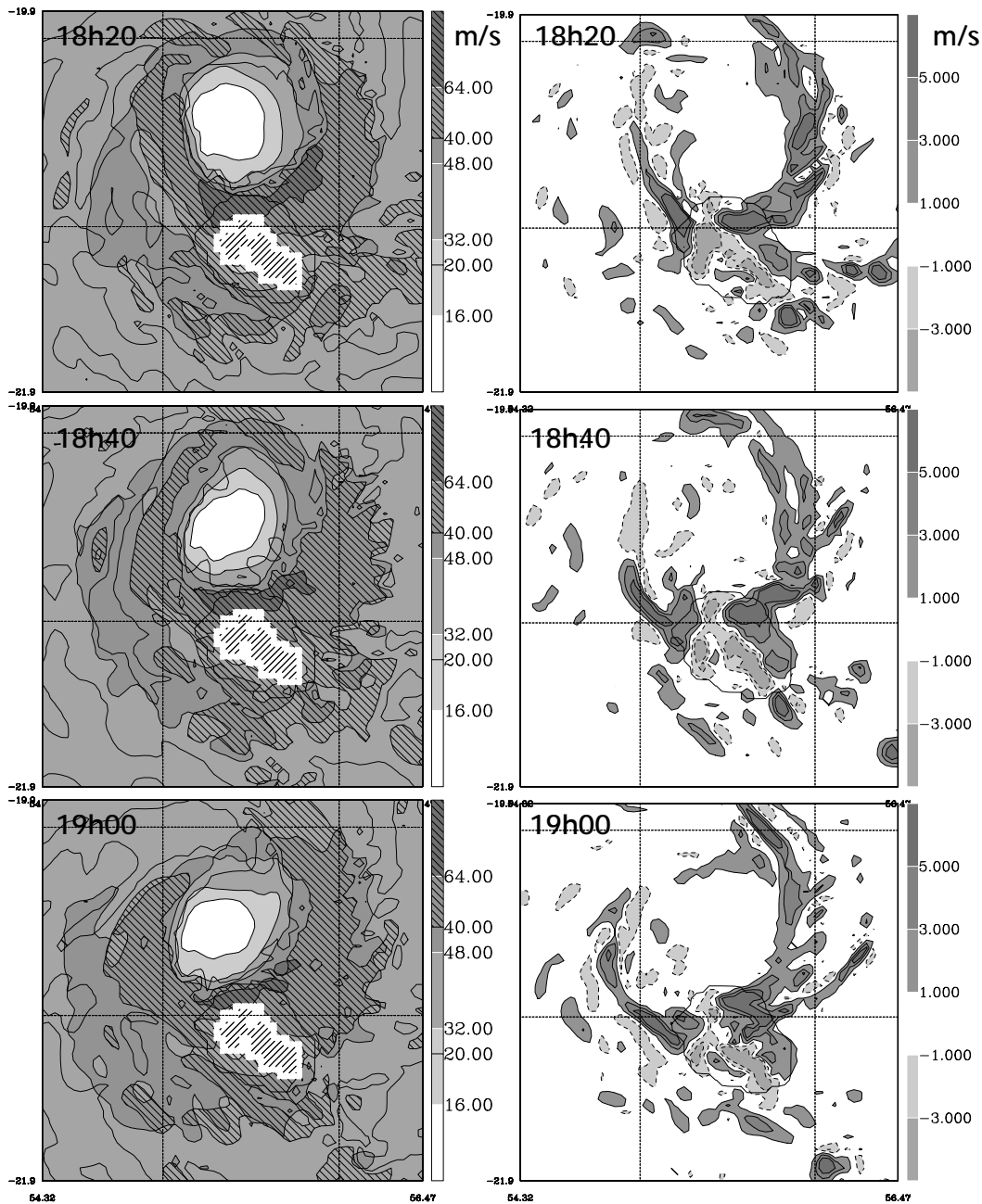
Fig. 11. Left panels: horizontal wind speed (shaded, m s^{-1}) and radar reflectivity (20 and 40 dBZ contours, hatched zones denote values >40 dBZ) from the 4-km model of experiment "*Island*" at 1000 m altitude, every 20 min from 18:20 to 19 h; right panels: as left panels, except for vertical velocity values (shaded, m s^{-1}) at 5000 m altitude.

the cyclonic flow passing around the island. The two elongated, east-northeast–west-southwest oriented, regions with low winds are observed in the immediate downwind side of the highest terrains, in the wake of the island.

A low reflectivity region is located downstream of the low-wind region whereas the maximum values are found over the island (Fig. 12). The secondary maxima at 50 to 100 km west of the island are also related to the horizontal convergence of

wind passing around the island. The vertical velocity field displays a maximum in the western part of the island, in the leeside (Fig. 12). This is a different situation from that displayed at an earlier time (Fig. 11), when only downward motions were observed there.

The steep topography of Réunion island has a strong influence on the wind field (Fig. 13). At 17 h (not shown) and 18 h when the vortex is relatively far from the island, the strongest
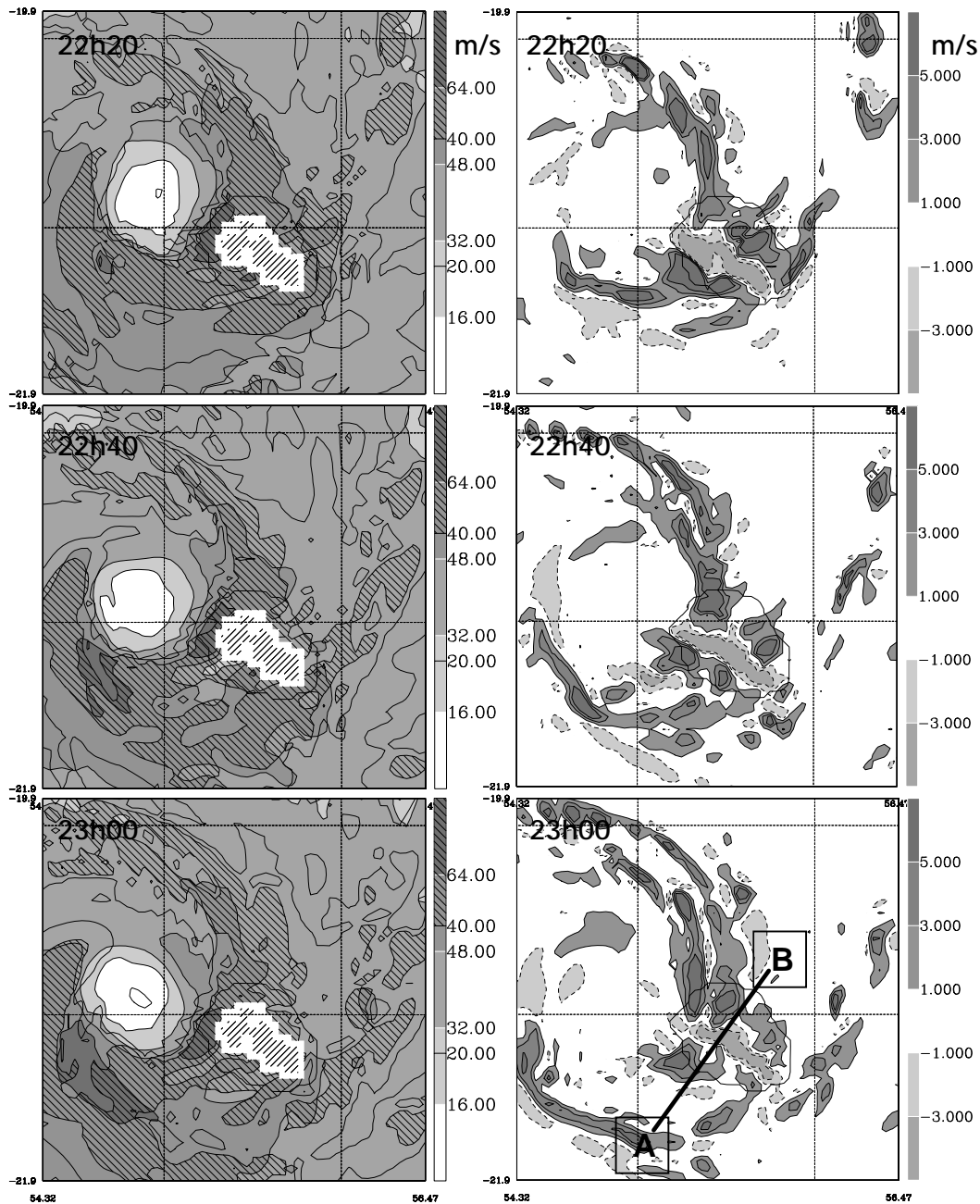
Fig. 12. As in Fig. 11, except for 22:20 to 23 h. Line AB in the lower right panel shows the location of the southwest–northeast vertical cross section in Fig. 13.

winds ($>64\,\mathrm{m\,s^{-1}}$) are located below an altitude of 2000 m on the upwind side of the island. At 20 h, when the eyewall is at the closest distance from Réunion island, the maximum winds move to the island above the highest peaks, up to 5000 m altitude. Until 24 h, the strongest winds stay over the central part of the island, while moving slightly downwind. This maximum is correlated with a mountain wave, characterised by weaker winds and downward motions above 8000 m altitude over the top of the island, then upward mo-

tions over the lee side. Indeed, the destruction of the Bras Sec forest ($0.65\,\mathrm{km^2}$) in Cilaos, over the southern high terrains of Réunion island, was probably caused by orographically enforced winds, amplified by sporadic gusts, blowing over the downwind slope. This development of strong orographic wave which can propagates upward might explain the observed second peak of convective inertia-gravity waves in the lower stratosphere after the passage of TC Dina near Réunion island (Chane Ming et al., 2010). Compared to "*Ocean*", the
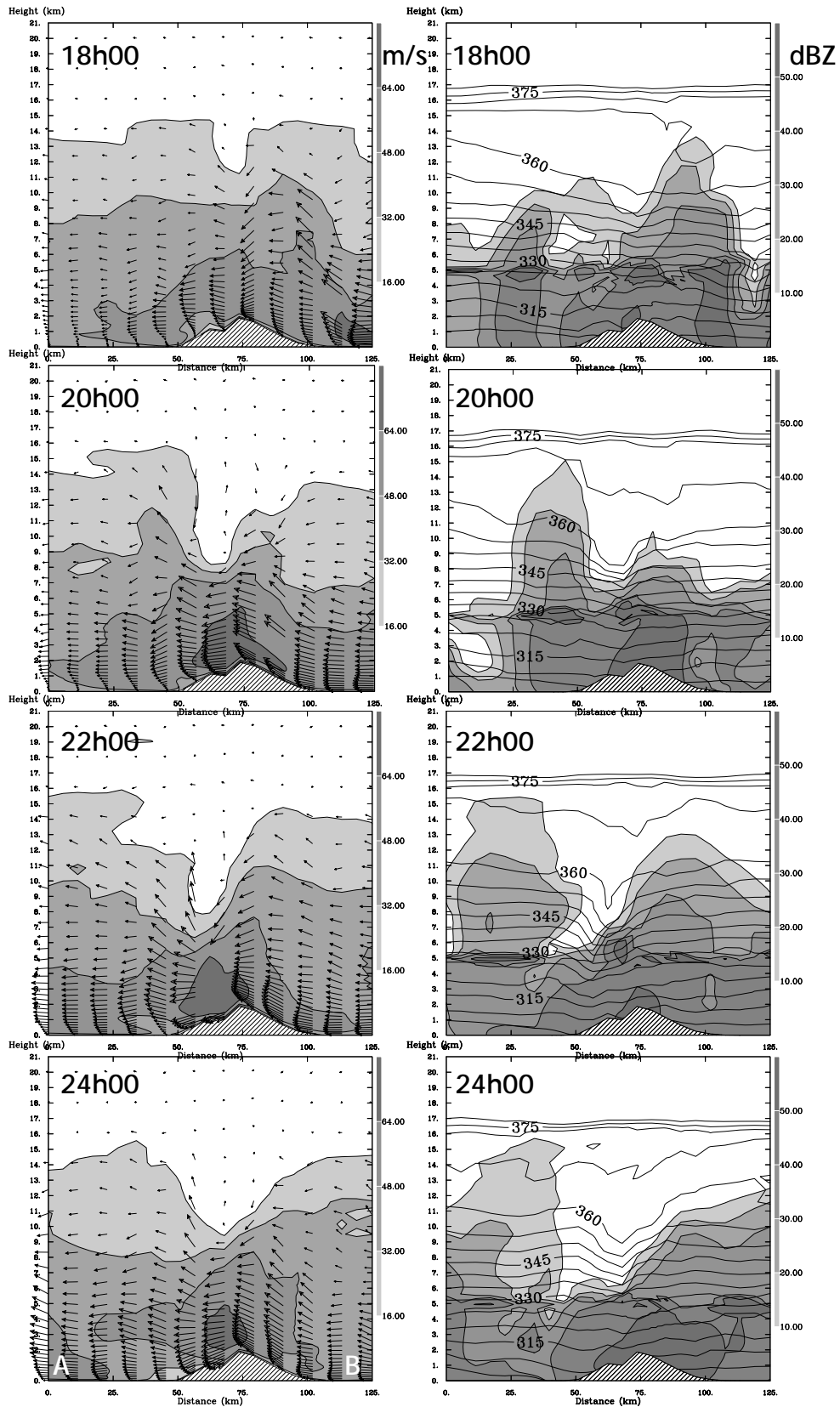
Fig. 13. Left panels: vertical cross-sections of horizontal wind speed (shaded, m s^{-1}) and wind vectors along line AB (see Fig. 12) in the 4-km model of experiment "*Island*", every 2 h from 18 to 24 h; right panels: as left panels, except for radar reflectivity (shaded, dBZ) and potential temperature (contours, K).
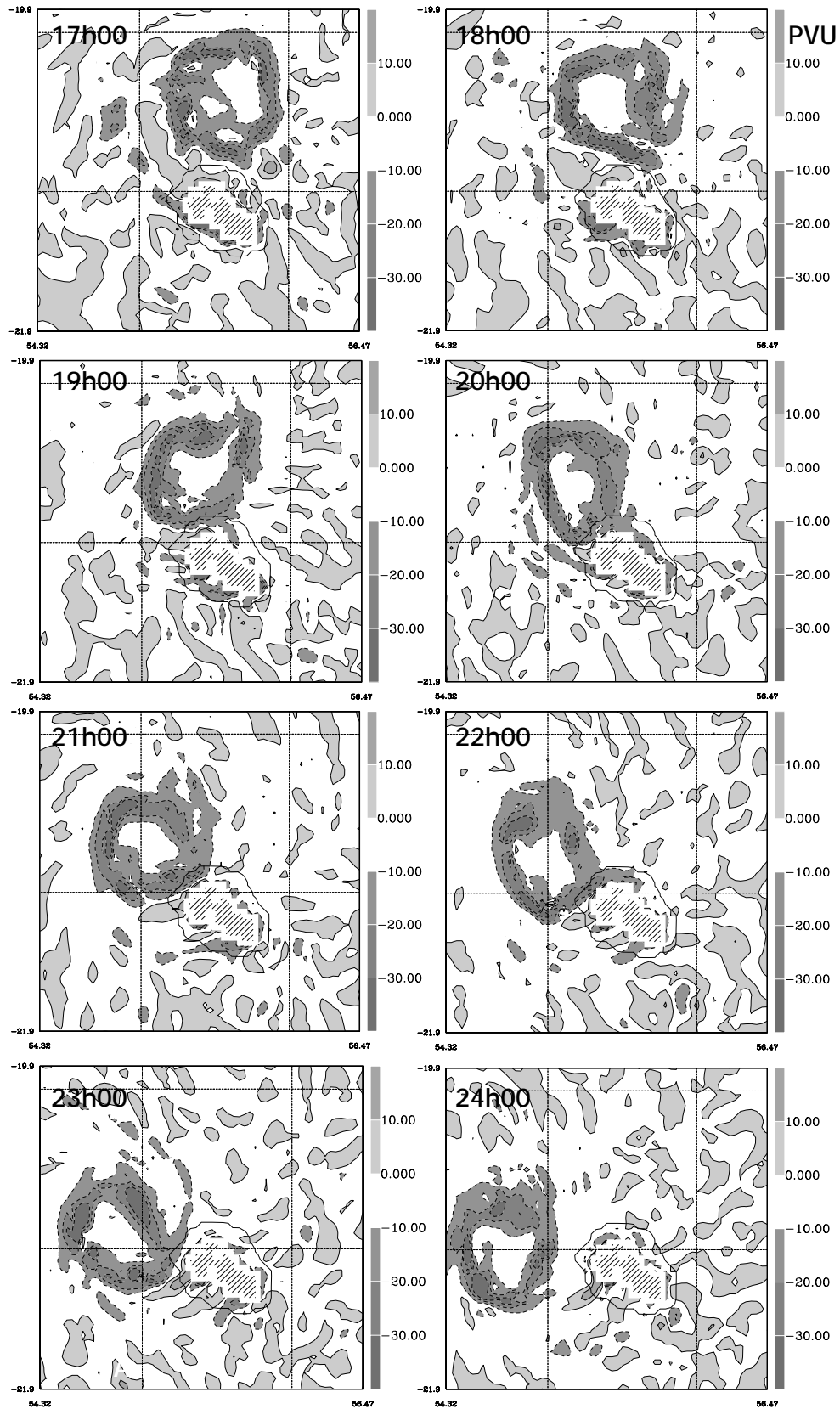
Fig. 14. Potential vorticity fields (shaded, PVU $= 10^{-6}\,\mathrm{m^2\,s^{-1}\,K\,kg^{-1}}$) from the 4-km model of the "*Island*" experiment at 1000 m altitude, every hour from 17 to 24 h.

distribution of winds is more stationary and has slightly more intense maxima, which certainly amplifies the local impact of the storm.

The highest radar reflectivity values are located along the upwind side of the island and hardly reach the downwind side (Fig. 13). The mountain wave strongly modulates the radar reflectivity field by inducing a substantial decrease after the top of the mountain in relation with downward motions aloft, and then an increase at some distance downwind where upward motions exist in altitude. This is significantly different from the "*Ocean*" experiment which had relatively more intense and more variable convective and stratiform precipitation. The presence of orographically induced stationary precipitation maxima over the upwind side of the island represents a potentially dangerous situation in terms of accumulated rain and associated runoff.

The orographic effect can also be identified on the potential vorticity (PV) field (= $\boldsymbol{\xi} \cdot \nabla\theta/\rho$, where $\cdot$ is the full three-dimensional scalar product, $\boldsymbol{\xi}$ is the vorticity vector, $\nabla\theta$ is the gradient of potential temperature θ and ρ is the air density) at 1000 m altitude (Fig. 14). Apart from the strong negative (cyclonic) values associated with the eyewall, the most interesting characteristic is the presence of alternately positive and negative PV bands. These "PV streamers" are similar, though on a smaller scale, to those observed in the lee side of an orographic barrier with individual peaks and passes, such as the Alps, when the synoptic wind flows in a direction perpendicular to the obstacle (Aebischer and Schär, 1998). Individual pairs of banners with positive and negative values of PV are related to flow splitting either on the scale of the whole massif (primary banners) or on that of individual peaks (secondary banners). As seen in Fig. 3b, the orography of Réunion island used for the numerical simulation at 4-km horizontal resolution is relatively simple with two regions above 2000 m altitude : Pîton des Neiges at northwest and Pîton de la Fournaise at southeast. In agreement with the direction of the cyclonic wind intercepting Réunion island, these PV banners extend northwest of the island at 17 and 18 h, west of it from 19 till 21 h, and toward southwest from 22 till 24 h. In relation with the relatively simple orography, a unique couple of negative and positive PV banners can be seen to the northwest at 17 and 18 h, when the two peaks are approximately aligned with the wind direction, whereas four of them are identified afterwards to the west and southwest when the wind blows more perpendicularly.

From 18 to 20 h, the decreasing intensity of cyclonic PV in the southern part of the eyewall probably results from an interaction with the orographically induced band of anticyclonic PV (light grey) which extends to the northwest of the island, over a distance decreasing from about 100 to 50 km. At 20 h, the cyclonic PV (dark grey) streamer which extends toward northwest over greater length begins to interact with the weakened southwestern part of the eyewall. Accordingly, as the storm propagates toward southwest after 20 h, this region builds up and intensifies again. After 21 h, the orography

of Réunion island, being exposed to northerly winds to the east of the storm, now generates cyclonic and anticyclonic PV streamers of 20 to 50 km length south of the island. But due to this south location they no longer interact with the dynamics of the distant eyewall. Due to the differences in island size and aspect as well as the non-direct landfall of TC Dina, this pattern can be analysed as a combination of the situation in Taiwan where the strongest typhoons are perturbed by, but pass around the island with a continuous track (e.g., Lin et al., 2006), and the situation in Luzon where Typhoon Zeb (1998) reformed and reintensified after a weakening phase when it passed over the terrain (Wu et al., 2003).

6 Control parameters

As discussed in Chen and Lin (2005), the characteristics of a moist flow over an orographic barrier depend on a moist Froude number defined as $F_w = U/(N_w h)$ where U is the basic horizontal wind speed, N_w is the moist Brunt-Väisälä frequency (= $g/\theta_{vm}d\theta_v/dz$, where g is the acceleration of gravity, θ_v the virtual potential temperature, θ_{vm} the mean virtual potential temperature in the considered layer, z the vertical coordinate) and h is the mountain height. When F_w is low (<1, "subcritical" regime), the flow is partially blocked or passes around the obstacle and rainfall is produced over the upwind side of the terrain. When F_w is moderate ($\approx$1, "critical" regime), a long lasting convective system is located in the vicinity of the mountain peak. When F_w is large (>1, "supercritical" regime), a propagating system develops on the downwind side of the barrier. When the basic wind speed (and F_w) increases and N_w is fixed, the flow tends to shift from one regime to another, i.e., from "flow around" to "flow over". This is what happens from 18 to 20 h (Fig. 13) when the most intense winds reach the island and move from the upwind side to the peak of the mountain. This is corroborated by the analysis of streamlines (not shown) which reveals that, before 18 h, air parcels in the lowest levels (below 500 m) pass around the elevated terrains whereas, from 18 to 20 h, they predominantly pass over. The presence of strong winds on the downwind side at 22 to 24 h is probably caused by the flow losing potential energy and accumulating kinetic energy as it decreases in size after the crest (Houze, 1993).

Vertical and horizontal Fourier transforms have been applied to the wind fields from 18 to 24 h, providing a spatial characterisation of the mountain wave over the top of the island. The derived horizontal and vertical wavelengths are 63 and 5 km, respectively. The natural vertical wavelength of the flow (= $2\pi U/N$, where N is the Brunt-Väisälä frequency) is 3.5 km (with $U = 5.5$ m s^{-1} and $N = 10.10^{-3}$ s^{-1}), smaller than the observed value of 5 km. When the natural wavelength of the flow is smaller than the observed one, resonance is still possible in the lower layers, the wave energy propagates upward and is absorbed in the upper levels (Gill, 1982). This is consistent with the propagation of the simulated wave

to the top of the domain (note, however, that a numerical "damping layer" is imposed in the uppermost part of the simulated domain, well above the tropopause level).

Although TC Dina did not cross Réunion island, the conceptual model of Lin et al. (2006) can be used to quantify the orographic effect on track. In our case, the non-dimensional flow parameters (V_{max}/Nh, U/Nh, R/L_y, U/fL_x, V_{max}/fR, $h/L_x = 2.279$, 0.195, 0.357, -2.264, -52.830, 0.061; where V_{max} is the maximum tangential wind, R the radius of V_{max}, f the Coriolis parameter and L_x and L_y the horizontal scales of the mountain in x and y-directions) would favour a continuous track, as observed in reality and in the "*Island*" experiment. Parameter $V_{max}/Nh(= 2.279)$ controls this continuity, while parameter $R/L_y(= 0.357)$ controls the direction of deviation. This deviation is larger in a case of weak cyclones, i.e., for small V_{max}/Nh parameters. Here it is necessary to change the north–south direction of Taiwan in Lin et al. (2006) to the northwest–southeast direction of Réunion island with a track perpendicular to the orography. In this configuration, even if V_{max}/Nh is large, which would theoretically induce a small southward deviation (in the Southern Hemisphere), R/L_y is small, which would theoretically induce a large northward deviation (in the Southern Hemisphere). This would agree with the observed northward deviation of Dina's track even though this deviation is small.

7 Concluding remarks

Both *"Ocean"* and *"Island"* experiments produce realistic TC characteristics in terms of rainfall, wind, intensity and structure, in agreement with the observations of TC Dina. Even though both simulated storms pass closer to the island than the actual one, the impact of the island on storm track is hardly detectable. Nevertheless, both simulations display significant differences in intensity and inner core dynamics during the interaction period which lasts from 15 to 24 h. During this period the presence of the island slows the intensification process of the TC and induces a less intense TC in "*Island*" compared to "*Ocean*" in terms of MSLP and maximum wind intensities. On the contrary, Chambers and Li (2011) showed an intensification of TC after passing the Hawaii's BI which is 4 times larger than Réunion island. The simulated storms also display different characteristics of their inner core dynamics. In "*Ocean*" the elliptical eyewall structures first rotate cyclonically from 15 to 20 h (O1), and then become steadier from 20 to 24 h (O2) with a more circular shape. In "*Island*" from 15 to 20 h (I1), the circular eyewall structures rotates at a speed slightly slower than in (O1), but then reaches a more stationary state from 20 to 24 h (I2) when the horizontal circulation appears to be largely controlled by orographic forcing.

By comparing (O1) and (I1), it appears that the orography of Réunion island damps the natural elliptical eyewall rota-

tion and forces a circular eyewall. This finding is similar to Chambers and Li (2011) who showed an axisymmetrisation of TC passing close to Hawaii's BI. A comparison between (O2) and (I2) shows that the orographic forcing at the closest distance between the storm and the island controls the horizontal circulation. Actually (O2) and (I2) are quite similar, suggesting that the major orographic forcing occurs when the TC approaches the island from 15 to 20 h. After 20 h the characteristics are similar in both simulations, with negligible influence of the island. The orography of Réunion island is not as detrimental to the cyclonic circulation as observed for some typhoons interacting with Taiwan (e.g., Lin et al., 2011) or Hawaii's BI (Chambers and Li, 2011). This overall weaker impact may be due to Dina and both simulated storms being intense TC and Réunion island being much smaller than Taiwan and Hawaii's BI. It is also interesting to note that although the orography has a substantial impact on the storm dynamics, in the "*Island*" experiment no vertical tilt of the TC centre (defined as the wind and pressure minimum) is observed showing no impact of the orography on the core vertical structure.

The evolution of the vertical structure of the cyclone (besides the inner core part) during the interaction period reveals the main forcing mechanisms associated with the presence of the island. Along the upwind side, the cyclonic flow slows down which induces horizontal convergence and upward vertical velocities. Then a strong orographic wave develops over the island peak, which modulates the wind components and reflectivity and might be a source of convective inertia-gravity waves in the lower stratosphere (Chane Ming et al., 2010). Finally there is subsidence at some distance on the downwind side, and horizontal winds and reflectivity values are weaker.

This study is being completed using a fourth domain centred on the island, with a higher horizontal resolution of 1 km. The goal is to further investigate the structure and evolution of the meso-γ scale structures of the eyewall in relation with the orographic forcing. The local impact of the cyclone, in terms of rainfall and wind intensity will also be more precisely analysed in relation with the complex small-scale topography of the island. For a more precise study on the effect of orography and especially on the distance of the influence of island, idealised simulations are needed to assess all parameters.

References

Aebischer, U. and Schär, C.: Low-level potential vorticity and cyclogenesis to the lee of the Alps, J. Atmos. Sci., 55, 186–207, 1998.

Barnes, S. L.: A technique for maximizing details in numerical weather map analysis, J. Appl. Meteor., 3, 396–409, 1964.

Bender, M. A. and Kurihara, Y.: A numerical study of the effect of the mountainous terrain of Japan on tropical cyclones, in: Short- and Medium-Range Numerical Weather Prediction, Collection of Papers Presented At WMO/IUGG NWP Symposium Tokyo, Japan, 4–8 August 1986, Geneva, Switz, World Meteorological Organization, 651–663, 1987.

Bender, M. A., Tuleya, R. E., and Kurihara, Y.: A numerical study of the effect of island terrain on tropical cyclones, Mon. Weather Rev., 115, 130–155, 1987.

Bougeault, P. and Lacarrère, P.: Parameterization of orography induced turbulence in a meso-beta scale model, Mon. Weather Rev., 117, 1870–1888, 1989.

Brand, S. and Blelloch, J. W.: Changes in the characteristics of typhoons crossing the Philippines, J. Appl. Meteor., 12, 104–109, 1973.

Braun, S. A.: A cloud-resolving simulation of hurricane Bob (1991): storm structure and eyewall buoyancy, Mon. Weather Rev., 130, 1573–1592, 2002.

Caniaux, G., Redelsperger, J. L., and Lafore, J. P.: A numerical study on the stratiform region of a fast moving squall line. Part II: Relationship between mass, pressure, and momentum fields, J. Atmos. Sci., 52, 331–352, 1995.

Caroff, P.: Saison cyclonique 2001/2002. Sainte Clotilde, La Réunion, France: Météo-France – Direction interrégionale de la Réunion, 96 pp., 2002.

Caroff, P. and Quetelard, H.: Dina: Cyclone tropical intense "Dina" à la Réunion. Sainte Clotilde, La Réunion, France: Météo-France – Direction interrégionale de la Réunion, 64 pp., 2002.

Chambers, C. R. S. and Li, T.: The Effect of Hawai'i's Big Island on Track and Structure of Tropical Cyclones Passing to the South and West, Mon. Weather Rev., 139, 3609–3627, 2011.

Chane Ming, F., Chen, Z., and Roux, F.: Analysis of gravity-waves produced by intense tropical cyclones, Ann. Geophys., 28, 531–547, doi:10.5194/angeo-28-531-2010, 2010.

Chang, S. W.-J.: The orographic effects induced by an island mountain range on propagating tropical cyclones, Mon. Weather Rev., 110, 1255–1270, 1982.

Chang, C.-P., Yeh, T.-C., and Chen, J. M.: Effects of terrain on the surface structure of typhoons over Taiwan, Mon. Weather Rev.,

121, 734–752, 1993.

Charnock, H.: Wind stress on a water surface, Quart. J. Roy. Meteor. Soc., 81, 639–640, 1955.

Chen, S.-H. and Lin, Y.-L.: Effects of moist Froude number and CAPE on a conditionally unstable flow over a mesoscale mountain ridge, J. Atmos. Sci., 62, 331–350, 2005.

Cuxart, J., Bougeault, P., and Redelsperger, J.-L.: A turbulence scheme for mesoscale and large eddy simulation, Q. J. Roy. Meteorol. Soc., 126, 1–30, 2000.

Gal-Chen, T. and Sommerville, R. C.: On the use of a Coordinate Transformation for the solution of the Navier-Stokes Equations, J. Comput. Phys., 17, 209–228, 1975.

Gill, A. E.: Atmosphere-Ocean dynamics, Academic Press, 662 pp., 1982.

Hebert, P.: Atlantic hurricane season of 1979, Mon. Weather Rev., 108, 973–990, 1980.

Hoarau, K.: L'influence du relief sur les vents d'un cyclone tropical. Le cas du cyclone Monique, La Météorologie, 34, 53–59, 2001.

Houze Jr., R. A.: Cloud dynamics, Academic Press, 573 pp., 1993.

Huang, Y.-H., Wu, C.-C., and Wang, Y.: The Influence of Island Topography on Typhoon Track Deflection, Mon. Weather Rev., 139, 1708–1727, 2011.

Jian, G.-J. and Wu, C.-C.: A numerical study of track deflection of Supertyphoon Haitang (2005) prior to its landfall in Taiwan, Mon. Weather Rev., 136, 598–615, 2008.

Kain, J. S. and Fritsch, J. M.: A one-dimensional entraining/detraining plume model and application in convective parameterization, J. Atmos. Sci., 47, 2784–2802, 1990.

Kain, J. S. and Fritsch, J. M.: Convective parameterization for mesoscale models: The Kain-Fritsch scheme. The Representation of Cumulus in numerical models, Meteor. Monogr., 46, 165–177, 1993.

Kurihara, Y., Bender, M. A., and Ross, R. J.: An initialization scheme of hurricane models by vortex specification, Mon. Weather Rev., 121, 2030–2045, 1993.

Kurihara, Y., Bender, M. A., Tuleya, R. E., and Ross, R. J.: Improvements in the GFDL hurricane prediction system, Mon. Weather Rev., 123, 2791–2801, 1995.

Lafore, J. P., Stein, J., Asencio, N., Bougeault, P., Ducrocq, V., Duron, J., Fischer, C., Héreil, P., Mascart, P., Masson, V., Pinty, J. P., Redelsperger, J. L., Richard, E., and Vilà-Guerau de Arellano, J.: The Meso-NH Atmospheric Simulation System. Part I: adiabatic formulation and control simulations, Ann. Geophys., 16, 90–109, doi:10.1007/s00585-997-0090-6, 1998.

Lin, C.-Y., Hsu, H.-M., Sheng, Y.-F., Kuo, C.-H., and Liou, Y.-A.: Mesoscale processes for super heavy rainfall of Typhoon Morakot (2009) over Southern Taiwan, Atmos. Chem. Phys., 11, 345–361, doi:10.5194/acp-11-345-2011, 2011.

Lin, Y.-L., Chen, S.-Y., Hill, C. M., and Huang, C.-Y.: Control parameters for the influence of a mesoscale mountain range on cyclone track continuity and deflection, J. Atmos. Sci., 62, 1849–1866, 2005.

Lin, Y.-L., Witcraft, N. C., and Kuo, Y.-H.: Dynamics of track deflection associated with the passage of tropical cyclones over a mesoscale mountain, Mon. Weather Rev., 134, 3509–3538, 2006.

Morcrette, J.-J.: Description of the radiation scheme in the ECMWF model. ECMWF Tech. Memo. 165, Research Department ECMWF, Reading, United Kingdom, 26 pp., available from European Centre for Medium-Range Weather Forecasts, Shin-

field Park, Reading, Berkshire RG2 9AX, UK, 1989.

Noihlan J. and Planton, S.: A simple parametrization of land surface process for meteorological models, Mon. Weather Rev., 117, 536–549, 1989.

Nuissier, O., Rogers, R. F., and Roux, F.: A numerical simulation of Hurricane Bret on 22–23 August 1999 initialised with airborne Doppler radar and dropsonde data, Q. J. Roy. Meteorol. Soc., 131, 155–194, 2005.

Oda, M., Nakanishi, M., and Naito, G.: Interaction of an assymmetric double vortex and trochoidal motion of a tropical cyclone with the concentric eyewall structure, J. Atmos. Sci., 63, 1069–1081, 2006.

Padya, B. M.: Spatial variability and gustiness of cyclone winds : Gervaise, Mauritius, February 1975, Austr. Metor. Mag., 23, 61–69, 1975.

Pan, C. J., Lai, H. C., Yang, S. S., Reddy, K. K., and Chang, S.-C.: Wind profiler radar investigation on typhoon-orography interaction, Geophys. Res. Lett., 35, L24812, doi:10.1029/2008GL036368, 2008.

Peng, L., Wang, S.-T., Shieh, S.-L., Cheng, M.-D., and Yeh, T.-C.: Surface Track discontinuity of tropical cyclones crossing Taiwan: A statistical study, Mon. Weather Rev., 140, 121–139, 2012.

Quetelard, H., Bessemoulin, P., Cerveny, R. S., Peterson, T. C., Burton, A., and Boodhoo, Y.: Extreme Weather: World-Record Rainfalls During Tropical Cyclone Gamede, B. Am. Meteor. Soc., 90, 603–608, 2009.

Roux, F., Chane-Ming, F., Lasserre-Bigorry, A., and Nuissier, O.: Structure and evolution of intense Tropical Cyclone Dina near La Réunion on 22 January 2002 : GB-EVTD analysis of single Doppler radar observations, J. Atmos. Oceanic Tech., 21, 1501–1518, 2004.

Wang, S.-T.: Prediction of the movement and strength of typhoons in Taiwan and its vicinity. Research Rep. 108, National Science Council, Taipei, Taiwan, 100 pp., 1980.

Wu, C.-C. and Kuo, Y.-H.: Typhoons affecting Taiwan: Current understanding and future challenges, B. Am. Meteorol. Soc., 80, 67–80, 1999.

Wu, C.-C., Chou, K.-H., and Cheng, H.-J.: Eyewall contraction, breakdown and reformation in a landfalling typhoon, Geophys. Res. Let., 30, 1887, doi:10.1029/2003GL017653, 2003.

Yeh, T.-C. and Elsberry, R. L.: Interactions of typhoons with the Taiwan orography. Part I: Upstream track deflections, Mon. Weather Rev., 121, 3193–3212, 1993.

Yeh, T.-C., Hsiao, L.-F., Chen, D.-S., and Huang, K.-N.: A study on terrain-induced tropical cyclone looping in East Taiwan: case study of Typhoon Haitang in 2005, Nat Hazards, doi:10.1007/s11069-011-9876-7, 2011.

Zehnder, J. A. and Reeder, M. J.: A numerical study of barotropic vortex motion near a large-scale mountain range with application to the motion of tropical cyclones approaching the Sierra Madre, Meteor. Atmos. Phys., 64, 1–19, doi:10.1007/BF01044127, 1993.

Zhao, K., Xue, M., and Lee, W.-C.: Assimilation of GBVTD-retrieved winds from single-Doppler radar for short-term forecasting of super typhoon Saomai (0608) at landfall, Q. J. Roy. Meteorol. Soc., 138, 1055–1071, doi:10.1002/qj.975, 2012.